

# High-Gain And High-Performance Power Converter For Space Thrusters Based On Electro spray Technology

Francisco José Blázquez-Plaza<sup>\*†</sup>, Andrés Barrado<sup>\*</sup> and Mick Wijnen<sup>\*</sup>

<sup>\*</sup>Power Electronics Systems Group, Universidad Carlos III de Madrid

<sup>\*</sup>IENAI Space S.L.

Leganés, Madrid, Spain

francisco.blazquez@ienai.space · andres.barrado@uc3m.es · mick.wijnen@ienai.space

<sup>†</sup>Corresponding author

## Abstract

Electrospray thrusters rely on a high voltage gain power converter for extracting and accelerating the ions producing thrust. Enhancement of the converter's efficiency in space applications is essential since it avoids oversizing the power generation or storage system and it mitigates issues related to the power losses heat dissipation. The paper presents the DCM Forward-Flyback converter integrated with two fifth-order Cockcroft-Walton voltage multipliers for generating positive and negative high-voltage rail for electro-spray thrusters. This topology has a reduced component count, is small in size, and is lightweight. Switching losses are minimized by implementing a valley-switching strategy to achieve ZVS. The theoretical analysis is validated with simulation and experimental results.

## 1. Introduction

Electrospray thrusters have become an attractive option for space propulsion in recent years due to their high efficiency and compact size. The electro-spray propulsion principle involves generating a high electric field to ionize a propellant and accelerate the resulting ions to produce thrust, which is possible thanks to needle-like features that concentrate the electric field at their tip. Electro-spray thrusters are particularly advantageous for micro and nano-satellite systems, where space and mass are limited or where the electrical power on board is limited to a few tens of Watts.<sup>1</sup> As a result, they have excellent potential for satellite propulsion, enabling both orbital and attitude control of the spacecraft and the emergence of new business models.<sup>2</sup>

The aim of this study is to introduce a new high-gain (over 200 times voltage amplification factor) and high-performance (over 90% efficiency) topology for electro-spray thrusters suitable for integration into the spacecraft.

In the field of electro-spray propulsion for space applications, ensuring the emitter tip's health and mitigating spacecraft charging issues are crucial concerns.<sup>3</sup> Since electro-spray thrusters have the ability to emit either positively or negatively charged ion beams, which has an important implication for charge neutralization, it may be possible to operate electro-spray thrusters without the need for an external cathode, in theory. By firing two separate thrusters, one providing a positive ion beam and the other a matching negative ion beam, it is possible to maintain a neutral charge on the spacecraft. This allows the thrusters to operate continuously without any interruptions due to charge buildup.<sup>3</sup> To address these challenges, the topology proposed includes two arrays of Cockcroft-Walton voltage multipliers (CW-VMR). Each of the arrays generates one of the polarities (positive, negative) simultaneously from the satellite power bus, enabling the application of opposite polarities to two different thrusters or arrays of thrusters.

Furthermore, achieving zero voltage switching (ZVS) is a critical factor in enhancing the performance and efficiency of this topology. The switching frequency and duty cycle must be adjusted to achieve the desired voltage gain while ensuring ZVS and, therefore, reducing the voltage-current product during the MOSFET turn-on transition. Specifically, the MOSFET must be turned on when the voltages across all parasitic capacitances have reached the "valley"<sup>4</sup> (local minimum) voltage level to minimize the undesired parasitic resonance caused by the parasitic capacitance in the converter's switching transient. This resonance leads to significant current stress on the switching devices, elevated levels of switching noise, and imposes constraints on the attainable switching frequency.

Section 2 of this paper provides a comprehensive description of the steady-state behavior of the converter. Section 3 presents the simulation and experimental results obtained, providing further insights into the behavior of the

## POWER CONVERTER FOR ELECTROSPRAY THRUSTERS

converter. Finally, in Section 4, the conclusions are presented, underscoring the practical implications of this study for the development of high-performance power converters for electrospray thrusters.

## 2. Steady-state analysis

In a previous study,<sup>5</sup> the ideal steady-state performance of the Forward-Flyback with Cockcroft-Walton Voltage Multiplier converter (FF-CW) in DCM was discussed. The impact of parasitic capacitances on the operating phases of the circuit was also addressed, particularly under high voltage and very low power conditions.<sup>4</sup> This paper presents the inclusion of a second Cockcroft-Walton voltage multiplier (CW-VMR) array, which was not previously considered in the original design, to achieve positive and negative high-voltage rails from the satellite power bus, analyzing the effects of the inclusion of the parasitic capacitances introduced by this second CW-VMR in the converter's equations.

Fig. 1 shows the Forward-Flyback converter with two fifth-order CW-VMR topology. The switch  $S_1$  (NMOS MOSFET) is controlled by a high-frequency PWM signal. The primary and secondary return paths eventually meet at the spacecraft chassis level, consequently, the same ground symbol has been used to simplify theoretical analysis.

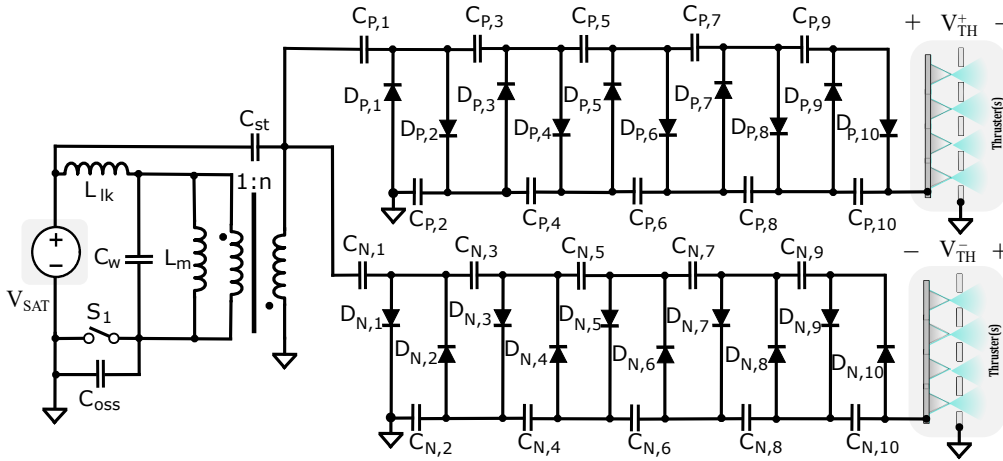


Figure 1: Forward-Flyback converter with two fifth-order CW-VMR considering the transformer non-idealities.

When the Flyback topology is combined with the CW-VMR, the converter operates differently from a conventional Flyback. In this combination, energy is delivered to the secondary side in two ways:

- **Forward energy transfer:** When the switch is ON and the transformer is magnetizing, some energy is also transferred to the secondary side, which charges the positive odd capacitors.
- **Flyback energy transfer:** When the switch turns off, the energy stored in the magnetizing inductance of the transformer is transferred to the secondary side, as in a conventional Flyback. This energy charges the even capacitors and provides power to the load.

In this converter, the effect of parasitic capacitances in the resonant operating phases and waveforms cannot be ignored. To obtain accurate results, it is crucial to model not only the MOSFET output capacitance ( $C_{oss}$ ) and the junction capacitances of the diodes ( $C_d$ ) but also the parasitic capacitances of the transformer, particularly important in very low-power thrusters since these parasitic components have a significant influence on the converter's behavior at low power. Therefore, leakage inductance ( $L_{lk}$ ), total winding parasitic capacitance ( $C_w$ ) and the equivalent stray capacitance ( $C_{st}$ ) are included in Fig. 1 together with magnetizing inductance ( $L_m$ ).

### 2.1 Voltage gain considering the voltage drop effects of the CW-VMR and DCM condition calculations.

Since the voltage drop in the CW-VM also affects the voltage gain, it must be considered. To understand the issue of voltage drop in the CW-VMR, it is important to consider the following concepts:

- During the Forward resonance (Section 2.2 - Interval 1), the odd capacitors are charged and their voltages depend on the voltage across the preceding even numbered capacitor, excluding the first capacitors ( $C_{P,1}$  and  $C_{N,1}$ ).

## POWER CONVERTER FOR ELECTROSPRAY THRUSTERS

- During the transformer demagnetization (Section 2.2 - Interval 4), the even capacitors are charged and their voltages depend on the voltage across the odd capacitors.

In order to charge the CW-VMR capacitors before delivering energy to the load, the current must flow through them. As a consequence, each consecutive capacitor (even capacitors) gets slightly discharged when they deliver energy to the load and when they charge the opposite branch of capacitors (odd capacitors), causing an undesirable voltage drop in the output.

It can be assumed that all CW-VMR capacitors are the same size (denoted in advance as  $C_{P,i} = C_{N,i} = C_{OUT}$ ) and are large enough to maintain a constant DC output voltage, the voltage drop across the diodes is negligible when compared to the voltage across the output capacitors, and the time it takes for the transformer to magnetize and demagnetize is approximately the same. Consequently, the output voltage drop ( $V_{DROP_{CW-VMR}}$ ) per CW-VMR is defined as the total voltage drop across the even capacitors in Eq. 1, which produces a voltage drop that adversely affects the voltage gain of the converter.<sup>4</sup> The number of voltage multiplier stages is defined as  $m$ , the switching frequency as  $f_{sw}$ , and the current delivered to the each output load as  $I_{OUT}$ .

$$V_{DROP_{CW-VMR}} = \left( \frac{2m^3 + 3m^2 + m}{12} \right) \cdot \frac{I_{OUT}}{f_{sw} C_{OUT}} \quad (1)$$

The ideal voltage gain for a single output is calculated in Eq. 2 and was presented in previous publications<sup>5</sup> for achieving a positive output. The voltage gain of this converter is influenced by several factors including the number of voltage multiplier stages ( $m$ ), the transformer's turn ratio ( $n$ ), the fraction of the period when the switch is on ( $D_1$ ), the magnetizing inductance ( $L_m$ ), the switching frequency ( $f_{sw}$ ), the output capacitance ( $C_{OUT}$ ) and the equivalent output resistance ( $R_{TH,P}$ ).

$$\frac{V_{TH}^+}{V_{SAT}}|_{ideal} = \frac{nm}{2} \cdot \left[ 1 + \sqrt{1 + \frac{2R_{TH,P}}{L_m f_{sw}} \cdot \left( \frac{D_1}{nm} \right)^2} \right] \quad (2)$$

If the single output assumptions are extrapolated to the two polarities version and assuming that the CW-VMR are ideal, the total voltage gain per output is still the number of CW-VMR stages ( $m$ ) by the transformer turn ratio ( $n$ ). However, the equivalent resistances from the thrusters appear in parallel.

It is assumed to achieve similar output voltages in both CW-VMR. Therefore, for the calculations it's assumed that  $V_{TH} \approx V_{TH}^+ \approx |V_{TH}^-|$  and the equivalent resistance is the parallel combination of both thrusters, the positive excited ( $R_{TH,P}$ ) with the negative excited ( $R_{TH,N}$ ) shown in Eq. 3.

$$R_{TH,eq} = \frac{R_{TH,P} \cdot R_{TH,N}}{R_{TH,P} + R_{TH,N}} \quad (3)$$

Therefore, the ideal gain of the dual output converter can be approximated as Eq. 4.

$$\frac{V_{TH}}{V_{SAT}}|_{ideal} = \frac{nm}{2} \cdot \left[ 1 + \sqrt{1 + \frac{2R_{TH,eq}}{L_m f_{sw}} \cdot \left( \frac{D_1}{nm} \right)^2} \right] \quad (4)$$

The real voltage gain is calculated including the voltage drop effects into the ideal voltage gain as expressed in Eq. 5. On this equation the converter overcomes the drop produced by the CW-VMR of each output while the equivalent load is now the parallel combination of both thrusters.

$$\frac{V_{TH}}{V_{SAT}}|_{ideal} = \frac{V_{TH} - V_{DROP_{CW-VMR}}}{V_{SAT}} \quad (5)$$

Consequently, the total voltage gain can be expressed as shown in Eq. 6.

$$\frac{V_{TH}}{V_{SAT}} = \frac{\frac{nm}{2} \cdot \left[ 1 + \sqrt{1 + \frac{2R_{TH,eq}}{L_m f_{sw}} \cdot \left( \frac{D_1}{nm} \right)^2} \right]}{1 + \frac{2m^3 + 3m^2 + m}{12R_{TH,eq} f_{sw} C_{OUT}}} \quad (6)$$

In addition,  $D_1$  is calculated using the expression of the voltage gain as shown in Eq. 7.

$$D_1 = \frac{nm}{2} \cdot \sqrt{\frac{2L_m f_{sw}}{R_{TH,eq}} \cdot \left( \left[ \frac{2V_{TH}}{nm V_{SAT}} \cdot \left( 1 + \frac{2m^3 + 3m^2 + m}{12R_{TH,eq} f_{sw} C_{OUT}} \right) - 1 \right]^2 - 1 \right)} \quad (7)$$

## POWER CONVERTER FOR ELECTROSPRAY THRUSTERS

Since the converter is expected to work in DCM,  $D_2$  is defined as the portion of the switching period corresponding to the demagnetization of the transformer but  $D_2 \neq 1 - D_1$ .

By ensuring that the magnetizing current ripple ( $\Delta i_{Lm}$ ) is equal during both the magnetizing and demagnetizing phases, Eq. 8 is obtained. Leakage inductance ( $L_{lk}$ ) has not been considered since the magnetizing inductance of the transformer ( $L_m$ ) is much greater than  $L_{lk}$ . Voltage drop has also assumed to be negligible.

$$\Delta i_{Lm} = \frac{V_{SAT} D_1}{L_m f_{sw}} \quad (8)$$

The average current through secondary is equal to  $mI_{OUT}$  in the ideal case. Therefore, the electric charge in steady-state across  $C_{P,1}$  ( $\Delta Q_{C_{P,1}}$ ) can be obtained as shown in Eq. 9, by calculating the integral of the demagnetization current since this capacitor is discharged with the forward energy transfer and charged with the flyback energy transfer.

$$\Delta Q_{C_{P,1}} = \int_{D_1/f_{sw}}^{1/f_{sw}} i_{sec}(t) dt = \frac{D_2 \Delta i_{Lm}}{2n f_{sw}} \quad (9)$$

$D_2$  is calculated next by substituting Eq. 8 into the previous system of equations:

$$D_2 = \frac{2nmL_m f_{sw} V_{TH}}{V_{SAT} D_1 R_{TH,eq}} \quad (10)$$

The magnetizing current ripple and the equivalent output load ( $R_{TH,eq}$ ) are connected through a specific value of magnetizing inductance, known as the critical value of  $L_m$  ( $L_{m,CRIT}$ ). When the magnetizing inductance is larger than  $L_{m,CRIT}$ , the current ripple is reduced below the limit of Discontinuous Conduction Mode (DCM), and the converter operates in Continuous Conduction Mode (CCM).

$$L_{m,CRIT} = \frac{V_{SAT} D_1 D_2 R_{TH,eq}}{2nm f_{sw} V_{TH}} \quad (11)$$

To ensure that converters consistently operate in DCM and avoid entering CCM, it is crucial to determine the worst-case scenario where the maximum voltage and frequency are applied to the minimum load. By confirming that this scenario operates in DCM, it can be inferred that the remaining operational points of the converter will also be in DCM. This approach guarantees the desired mode of operation throughout the converter's operating range.

## 2.2 Operation Intervals

There are six operation intervals, shown in Fig. 9, which are described below. Additionally, energy flow diagrams are provided for each interval. In these diagrams, black indicates that a component is inactive, blue indicates that it is active, and light blue indicates that it is active through its parasitic components.

- **Interval 1. Forward resonance ( $t_0$  to  $t_1$ ):** During the first interval of operation in a Forward-Flyback Converter, the MOSFET is turned on and energy is stored in the magnetizing inductance of the transformer ( $L_m$ ), which is known as the "Flyback energy". At the same time, the positive output odd-numbered and negative output even-numbered "Forward diodes" in the circuit become forward-biased and the odd capacitors are charged, which is referred to as "Forward energy". The forward diodes become forward-biased sequentially, and the next diode is only polarized once the corresponding odd capacitor is fully charged. The sum of the currents through the forward diodes is equal to the forward resonant current in the secondary circuit. The resonant output capacitance referred to the primary side of the transformer is defined as  $C_r$ .

$$C_r = 2n^2 \frac{C_{OUT}}{m} \quad (12)$$

The capacitance of the transformer winding ( $C_w$ ) and the stray capacitance referred to the primary circuit ( $C'_{st}$ ) are so small compared to the capacitance of the output capacitor ( $C_r$ ) that they can be ignored. Additionally, the magnetizing inductance of the transformer ( $L_m$ ) is much greater than the leakage inductance ( $L_{lk}$ ). As a result, the Forward resonant frequency ( $\omega_{for}$ ) for this interval of operation can be calculated as shown in Eq. 13.

$$\omega_{for} = \frac{1}{\sqrt{L_{lk} C_r}} \quad (13)$$

## POWER CONVERTER FOR ELECTROSPRAY THRUSTERS

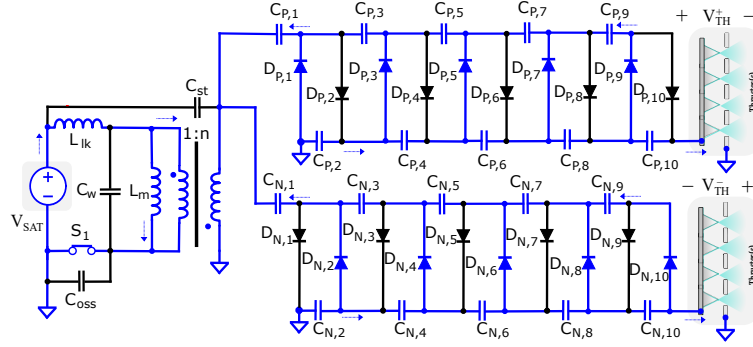


Figure 2: Energy flow during interval 1.

- **Interval 2.** ( $t_1$  to  $t_2$ ): This operating interval only happens when the MOSFET is turned on for a duration longer than the forward resonant semiperiod (Eq. 14). During this phase, the energy from the forward converter is transferred to the odd capacitors, causing the resonant current through the secondary ( $I_{sec}$ ) to decrease to zero. Once this happens, the MOSFET remains turned on and continues to store the Flyback energy in the magnetizing inductance. During this operating stage, there is a resonant current overlapped with the waveforms that does not affect the performance of the converter.

$$\frac{D_1}{f_{sw}} > \frac{t_{for}}{2} \quad (14)$$

Therefore  $t_{for} = t_2 - t_0$  can be obtained using Eq. 15 and depending if the duty cycle comply with Eq. 14 the waveforms will have a resonant current overlapped or not during  $t_2 - t_1$ .

$$t_{for} = 2\pi \sqrt{L_{lk} C_r} \quad (15)$$

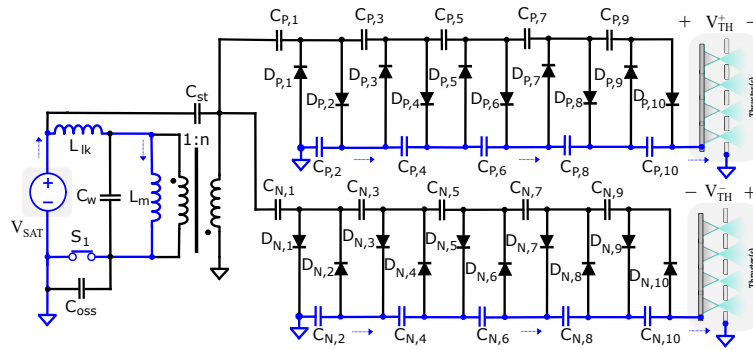


Figure 3: Energy flow during interval 2.

- **Interval 3. Slow-Voltage-Transition (SVT)** ( $t_2$  to  $t_3$ ): When the MOSFET is turned off, the parasitic capacitances in the circuit need to be charged before the Flyback energy can be transferred to the CW-VMR. The charging of these capacitances is accomplished by utilizing the energy stored in the magnetizing inductance. However, this charging process is not immediate, since the total parasitic capacitance ( $C_{par}$ ) is relatively large. As a result, the transition from MOSFET off to the delivery of Flyback energy to the CW-VM is not instantaneous.  $C_d$  is defined next as the addition of the parasitic capacitances of the CW-VMR diodes.

$$C_{par} = C_w + n^2 C_{st} + 4n^2 m C_d + C_{oss} \quad (16)$$

The equivalent circuit corresponding of the parasitic resonance to this operating stage is depicted in Fig. 4.

## POWER CONVERTER FOR ELECTROSPRAY THRUSTERS

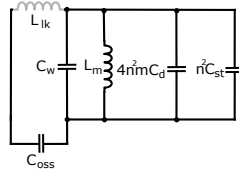


Figure 4: Equivalent circuit of the parasitic resonance during interval 3.

The resonance between  $L_m$  and  $C_{par}$  during the SVT is defined as "parasitic resonance"(where  $L_{lk}$  is assumed negligible). The parasitic resonant frequency ( $\omega_{par}$ ) is calculated next:

$$\omega_{par} = \frac{1}{\sqrt{L_m C_{par}}} \quad (17)$$

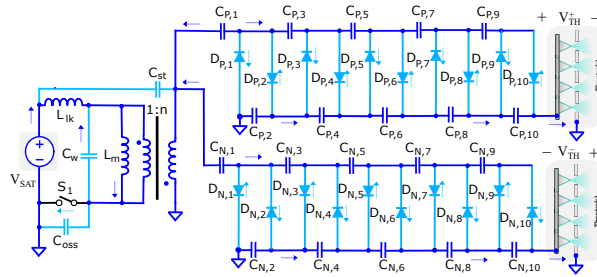


Figure 5: Energy flow during interval 3.

- **Interval 4.** ( $t_3$  to  $t_4$ ): After the SVT process is completed, the positive output even-numbered and the negative output odd-numbered diodes become forward-biased, resulting in the demagnetization of the transformer. During this demagnetization, the energy that was previously stored in the magnetizing inductance cause the odd capacitors to become charged.

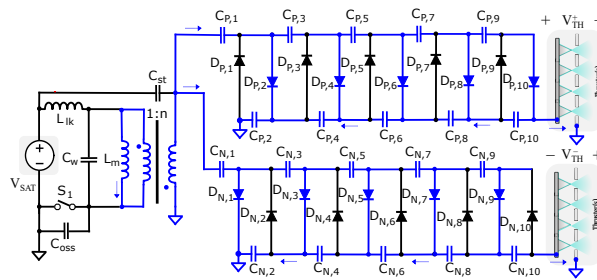


Figure 6: Energy flow during interval 4.

- **Interval 5.** ( $t_4$  to  $t_5$ ): Once the transformer has been demagnetized, all the diodes in the circuit are turned off, and a new resonant interval begins. The resonant frequency during this interval is the same as the parasitic capacitance frequency, which is denoted by  $\omega_{par}$ . This particular operating interval is referred to as the valley-switching operation.

To achieve ZVS (Zero Voltage Switching), it is necessary to turn ON the MOSFET when the voltage across all parasitic capacitances has reached the minimum voltage levels in this interval. By referring to the  $V_{DS}$  waveform shown in Fig. 9, the MOSFET should be turned ON when the minimum of the resonance is reached. This allows for the resonant energy to flow through the parasitic capacitances and magnetizing inductance to be conserved. The reduction in power losses also leads to an increase in the efficiency of the converter, resulting in a higher overall efficiency. The soft-switching technique also allows for higher switching frequencies to be used, which can lead to smaller and lighter passive components such as inductors and capacitors, resulting in a more compact converter design.

## POWER CONVERTER FOR ELECTROSPRAY THRUSTERS

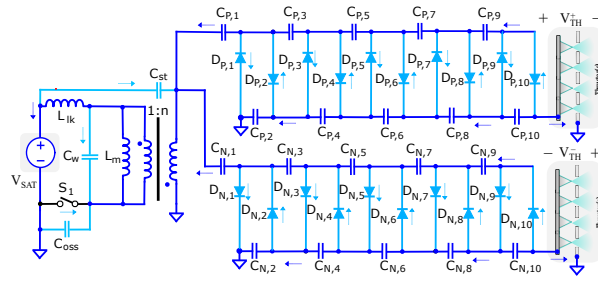


Figure 7: Energy flow during interval 5.

- Interval 6. ( $t_5$  to  $t_6$ ):** The MOSFET is just turned ON, the parasitic capacitances in the circuit are effectively short-circuited. As a consequence, a discharge current is demanded by these capacitances, which is proportional to their capacitance value and the voltage across them at time  $t = t_5$ . However, since the initial condition of the current through the leakage inductance at  $t = t_0$  (equal to  $I_{DS}$ ) is not zero, the waveforms during the first interval become distorted if ZVS is not achieved at the end Interval 5, and extra energy is needed at this interval. The energy required to perform this quasi-ZVS operation depends on the value of the parasitic capacitances and the voltage across them when the MOSFET is turned ON.<sup>4</sup>

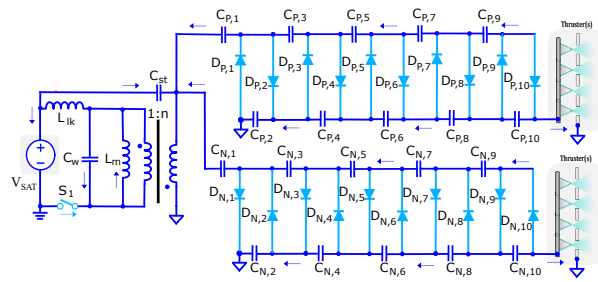


Figure 8: Energy flow during interval 6.

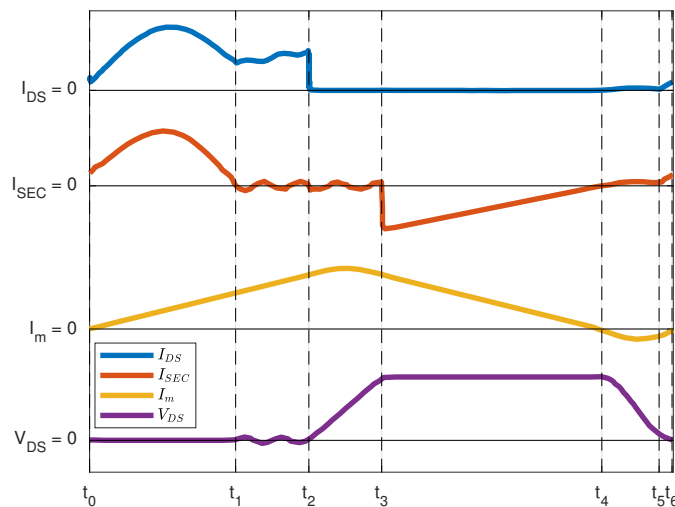


Figure 9: Waveforms of the converter in DCM: MOSFET current (blue), transformer secondary current (red), magnetizing current (yellow) and MOSFET drain-source voltage (purple).

### 3. Validation and experimental results

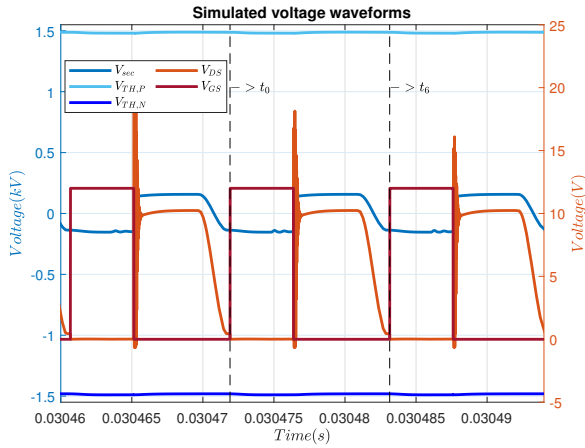
#### 3.1 Simulation

Simulations are presented in this section to validate the steady-state analysis carried out in the previous section. The specifications used in the simulations are presented in Table 1. The worst case, where the maximum voltage ( $\pm 1.5kV$ ) and power (10W) are achieved, has been chosen for simulation. The simulation has been carried out implementing the circuit shown in Fig. 1 in SIMETRIX. The simulation models for the components are the ones which correspond to the prototype board components, defined in next section on Table 2.

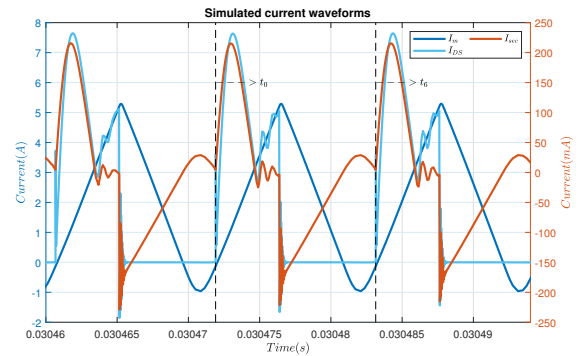
Fig. 10 displays the simulated steady-state waveforms to confirm the accuracy of the circuit's model. The similarity between the waveforms in Fig. 9 and Fig. 10 demonstrates a precise correlation between theoretical analysis and simulations. Theoretically, it is possible to turn on the mosfet in any of the resonance valleys. However, in the simulation, the voltage across the MOSFET's drain-source is monitored to switch at the first resonant valley voltage.

Table 1: Simulation specifications & Efficiency and power loss breakout report

Simulation specifications			Efficiency and power loss breakout report		
Parameter	Symbol	Value	Parameter	Symbol	Value
Input voltage	$V_{SAT}$	5V	Input power	$P_{IN}$	10.0359W
Output voltage	$V_{TH,P}$	1.5kV	Output power (positive output)	$P_{TH,P}$	4.90383W
	$V_{TH,N}$	-1.5V	Output power (negative output)	$P_{TH,N}$	4.89876W
Output power (per output)	$P_{TH,P}$	5W	Efficiency	$\frac{P_{TH,P}+P_{TH,N}}{P_{IN}}$	97.68%
Transformer turn ratio	$n$	30	Dissipated Power	$P_{LOSS}$	233.325mW
CW-VMR stages (per output)	$m$	5			



(a) Simulated voltage waveforms.



(b) Simulated current waveforms.

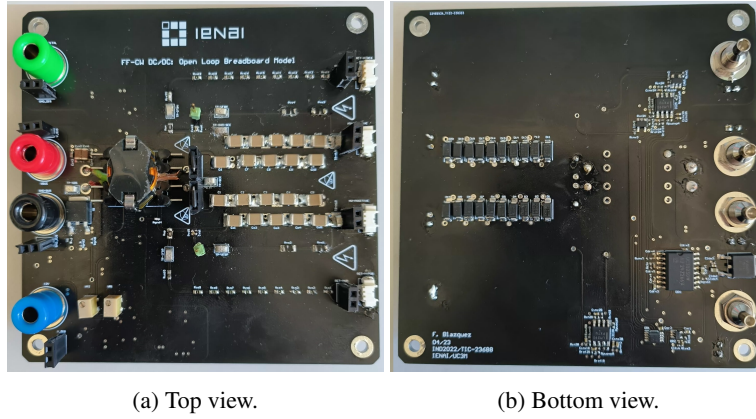
Figure 10: Converter's transient simulation.

Table 1 also presents the efficiency and power loss breakout report, where it can be observed the impact of zero-voltage switching (ZVS) on the converter's efficiency. The obtained results indicate an efficiency of 97.68% in the simulation. It should be noted that these measurements do not include losses incurred in the gate driver.

#### 3.2 Experimental results

A Forward-Flyback converter prototype featuring dual fifth-order CW-VMR was developed and tested to validate the theoretical analysis. The open loop prototype was implemented on a printed circuit board (PCB), as shown in Fig. 11. The transformer measurements and components used in the prototype are listed in Table 2. These components were carefully selected to ensure accurate and reliable testing of the converter. The prototype was enhanced with additional components to enable triggering of the MOSFET gate using a PWM signal, and to vary of the PWM's duty and frequency.

## POWER CONVERTER FOR ELECTROSPRAY THRUSTERS



(a) Top view.

(b) Bottom view.

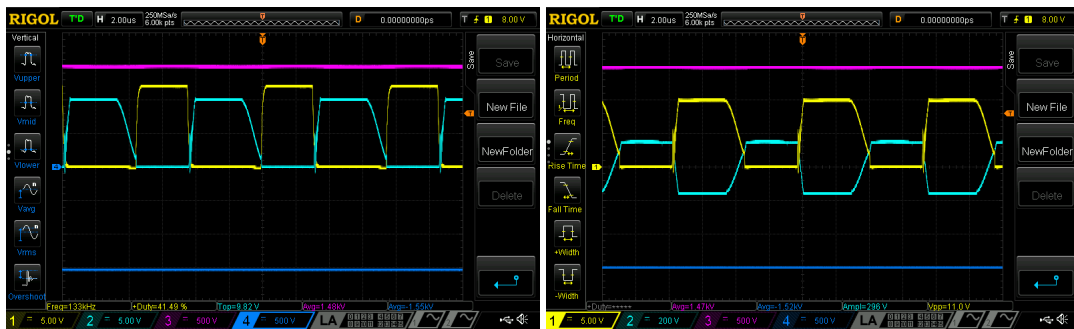
Figure 11: Converter's open loop prototype PCB.

Table 2: Open loop prototype: component listing

Ad-hoc RM6 Transformer Specifications			Components reference		
Parameter	Symbol	Value	Component	Identifier	Reference
Magnetizing inductance	$L_m$	$4.4\mu H$	MOSFET	$S_1$	IRFR7446TRPBF
Leakage inductance	$L_{lk}$	$75nH$	CW-VMR Diodes	$D_{P,1} - D_{P,10}$ $D_{N,1} - D_{N,10}$	GCJ43DR7LV224KW01K
Winding capacitance	$C_w$	$19.78nF$	CW-VMR Capacitors	$C_{P,1} - C_{P,10}$ $C_{N,1} - C_{N,10}$	BYG23M
Stray capacitance	$C_{st}$	$17.47nF$			

To evaluate the performance of the converter, the drain-source voltage and the gate-source voltage of the MOSFET are measured in the prototype in Fig. 12a. Additionally, the secondary voltage along with both output voltages are also measured in 12a. The converter exhibited stable and reliable performance, with waveforms that closely matched our theoretical predictions when comparing Fig. 10 with Fig. 12. The voltage at the secondary ( $V_{SEC}$ ) is inverted in comparison to the simulation results due to the difference in the reference point from which it was measured.

To achieve zero voltage switching (ZVS), it is crucial to turn ON the MOSFET when the voltages across all parasitic capacitances have reached the "valley" voltage levels. By referencing the drain-source voltage waveform, the MOSFET can be turned ON at the first resonance valley. Hence, it is necessary to adjust both the switching frequency and duty cycle to achieve the desired voltage gain of the converter while ensuring ZVS.



(a)  $C_1(\text{Yellow}) = V_{GS}$ ,  $C_2(\text{Light - Blue}) = V_{DS}$ , (b)  $C_1(\text{Yellow}) = V_{DS}$ ,  $C_2(\text{Light - Blue}) = V_{SEC}$ ,  
 $C_3(\text{Purple}) = V_{OUT,P}$ ,  $C_4(\text{Dark - Blue}) = V_{OUT,N}$        $C_3(\text{Purple}) = V_{OUT,P}$ ,  $C_4(\text{Dark - Blue}) = V_{OUT,N}$

Figure 12: Converter's oscilloscope waveforms.

The performance of the converter was evaluated under various operating conditions by conducting tests at different output voltages and output powers while measuring input voltage, output voltage, and input current to calculate the converter's efficiency. To ensure accurate measurements, the voltage applied voltages values to the loads were kept constant for each measured point, and each point was run by a time much longer than the settling time of the initial startup transient of the converter before taking the measurement. The output power was calculated based on the output voltage and load resistance values. Different loads for each output were used, ranging from  $400k\Omega$  to  $2M\Omega$  in steps of  $200k\Omega$ . One of the PCB which contains the test loads is shown in Fig. 13. These PCBs are capable of working at high voltage conditions. The output voltage was stepped from 1kV to 1.5kV in steps of 100V.

## POWER CONVERTER FOR ELECTROSPRAY THRUSTERS

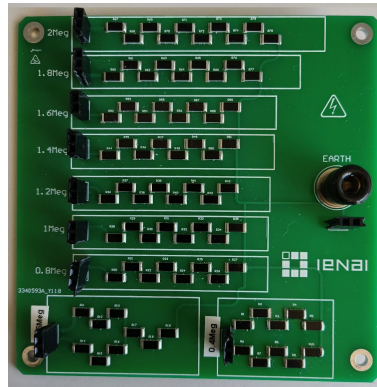
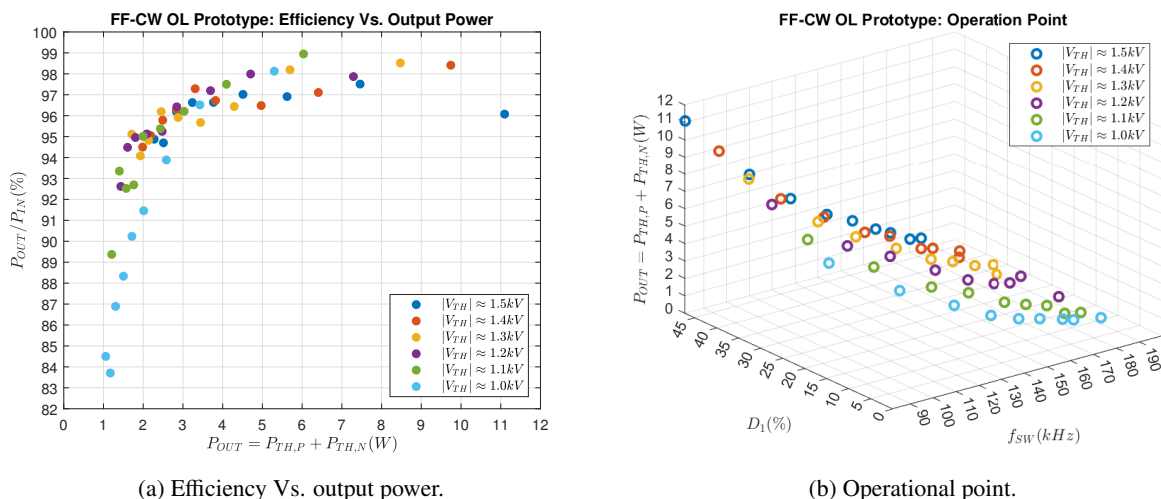


Figure 13: Converter's test loads PCB.

The efficiency plot of the converter can be observed in Fig. 14a, which displays the increasing output power values. The limited discretization of test loads restrict the range of power outputs that can be tested or measured accurately using the current version of the PCB of Fig. 13. This implies that the available values on the PCB do not cover the entire range from 1W to 10W for each output voltage. The efficiency shown in Fig. 14a corresponds to the power stage of the circuit illustrated in Fig. 1 and these measurements do not include losses incurred in the gate driver. The input voltage remains fixed at 5V.

The efficiency plot of the converter demonstrates a tendency of over 95% from 2W to 10W output, which outperforms the reported efficiencies of 85.57%,<sup>6</sup> 80.4%<sup>7</sup> and 88.5%<sup>8</sup> of different converters for electrospray propulsion. This, in combination with achieving such high conversion rates, make the proposed converter to fit with electrospray propulsion and proves to be a highly effective and a energy-efficient solution for powering small-scale spacecraft and satellites.

Additionally, Fig. 14b includes the operational point of frequency and duty cycle where the optimal valley-switching operation is achieved in every case and the optimal steady-state operating points are calculated following an iterative approach. The duty versus switching frequency curves demonstrate a predominantly linear relationship, although they do not align perfectly as a straight line. This slight deviation can be attributed to the inherent variability of the system's components, which are influenced by the voltage, temperature and the current flowing through them at each operating point. Therefore in future versions, the loop should be closed considering the variability of the valley-switching operation and turning the MOSFET ON at the minimum resonant valley voltage after the demagnetization of the transformer, in simple terms, monitoring the MOSFET drain-source voltage ( $V_{DS}$ ) to detect the resonant valley voltage and recomputing the switching frequency and duty cycle each period.



(a) Efficiency Vs. output power.

(b) Operational point.

Figure 14: Converter's open loop power stage prototype results.

## 4. Conclusions

This paper contributes to the field of electrospray propulsion technology by presenting a highly efficient and adaptable converter that supports dual thruster operation, which is needed to be able to emit a neutral beam. These findings have implications for the development of more effective and reliable propulsion systems for spacecraft.

Firstly, an adapted version of the converter topology presented in previous publications is proposed to obtain two outputs of opposite polarity and enabling the use of this topology in electrospray applications. This novel approach builds upon the previous work and incorporates updated mathematical equations, which have been redefined to represent the converter presented in this article. Notably, these equations are aligned with the simulation and prototype results, which are consistent, ensuring the desired output is achieved. Secondly, the hardware prototype of the converter was implemented and tested for various input voltages and output powers, demonstrating an overall efficiency of over 95% from 2W to 10W. The experimental prototype is able to achieve a voltage amplification factor of 300 (when  $V_{TH} = 1500$  and  $V_{IN} = 5$ ) for each output without an efficiency penalization.

The proposed topology has a low component count (only needing one MOSFET, a transformer and some CW-VMR stages) and can be adapted to any desired voltage range by incorporating additional CW-VMR stages. By ensuring the DCM condition in all operating points, it is possible to vary the output voltage and, therefore, being able to produce different thrust levels and specific impulses depending on the satellite needs.

Future work includes a detailed analysis of the control stage design since the optimal valley-switching operation needs the MOSFET to be turned ON at the minimum resonant valley voltage, which imply to design a valley-detector circuitry within a variable frequency control scheme. In addition, the capability of providing an alternating voltage to each thruster to prevent electrochemical degradation of the ionic propellant will be studied.

## 5. Acknowledgments

Sponsored by "Comunidad de Madrid" and the research project IND2022/TIC-23688.

## References

- [1] J. Mueller, R. Hofer and J. Ziemer, "Survey of propulsion technologies applicable to cubesats", Presented at 57th JANNAF Propulsion Meeting, 2010. [ONLINE] Available: <https://hdl.handle.net/2014/41627>
- [2] A. R. Tummala and A. Dutta, "An Overview of Cube-Satellite Propulsion Technologies and Trends", Aerospace, vol. 4, no. 4, p. 58, Dec. 2017, doi: 10.3390/aerospace4040058
- [3] F. Hicks, "Spacecraft charging and attitude control characterization of electrospray thrusters on a magnetically levitated testbed", Ph.D. dissertation, Space Propulsion Lab., Massachusetts Institute of Technology, Cambridge, MA, USA, 2017.
- [4] J. A. Serrano, P. Alou and J. A. Oliver, "DCM Forward-Flyback converter with Cockcroft-Walton Voltage Multiplier: steady-state analysis considering the influence of the parasitic capacitances at very low power and very high voltage gain", 2019 IEEE Energy Conversion Congress and Exposition (ECCE), Baltimore, MD, USA, 2019, pp. 6841-6847, doi: 10.1109/ECCE.2019.8911903.
- [5] M. S. Dall'Asta, V. B. Fuerback and T. Brunelli Lazzarin, "DCM forward-flyback converter integrated with a 5-order cockcroft-walton voltage multiplier: A steady-state and resonant current analysis", 2017 Brazilian Power Electronics Conference (COBEP), Juiz de Fora, Brazil, 2017, pp. 1-6, doi: 10.1109/COBEP.2017.8257407.
- [6] B. P. Baddipadiga, S. Strathman, M. Ferdowsi and J. W. Kimball, "A high-voltage-gain DC-DC converter for powering a multi-mode monopropellant-electrospray propulsion system in satellites," 2018 IEEE Applied Power Electronics Conference and Exposition (APEC), San Antonio, TX, USA, 2018, pp. 1561-1565, doi: 10.1109/APEC.2018.8341224.
- [7] I. F. Stelwagen, M. J. C. De Jong, W. Xu, R. Visee, E. Grustan-Gutierrez, O. Redwood, J. Huh, H. Gray, V. Giannetti, L. Liljeholm, T. Grnland, and J. P. W. Stark, "Development of a high-performance low-cost ppu for an electrospray colloid electric propulsion system for small satellite applications", in Proceedings of the International Astronautical Congress, IAC, vol. 2018-October, 2018.
- [8] D. Krejci, F. Mier-Hicks, C. Fucetola, P. Lozano, A. Hsu, and F. Martel, "Design and characterization of a scalable ion electrospray propulsion system", in IEPC-2015-149 34th International Electric Propulsion Conference, 07 2015.